

# Clock-jitter reduction in LISA time-delay interferometry combinations

Olaf Hartwig

*Max-Planck-Institut für Gravitationsphysik (Albert-Einstein-Institut), Callinstraße 38, 30167 Hannover, Germany*

Jean-Baptiste Bayle

*Jet Propulsion Laboratory, California Institute of Technology,  
4800 Oak Grove Drive, Pasadena, CA 91109, USA*

(Dated: June 9, 2021)

The Laser Interferometer Space Antenna (LISA) is a European Space Agency mission that aims to measure gravitational waves in the millihertz range. The three-spacecraft constellation forms a nearly-equilateral triangle, which experiences flexing along its orbit around the Sun. These time-varying and unequal armlengths require to process measurements with time-delay interferometry (TDI) to synthesize virtual equal-arm interferometers, and reduce the otherwise overwhelming laser frequency noise. Algorithms compatible with such TDI combinations have recently been proposed in order to suppress the phase fluctuations of the onboard ultra-stable oscillators (USO) used as reference clocks.

In this paper, we propose a new method to cancel USO noise in TDI combinations. This method has comparable performance to existing algorithms, but is more general as it can be applied to most TDI combinations found in the literature. We compute analytical expressions for the residual clock noise before and after correction, accounting for the effect of time-varying beatnote frequencies, previously neglected. We present results of numerical simulations that are in agreement with our models, and show that clock noise can be suppressed below required levels. The suppression algorithm introduces a new modulation noise, for which we propose a partial mitigation. This modulation noise remains the limiting effect for clock-noise suppression, setting strict timing requirements on the sideband generation.

## I. INTRODUCTION

The Laser Interferometer Space Antenna (LISA) is a European Space Agency (ESA) scientific space mission, which aims to measure gravitational waves (GWs) in the millihertz range [1]. Those waves are predicted by Einstein's theory of general relativity and produced by the quadrupolar moment of very dense objects, such as black hole binaries or coalescing super-massive black holes. The detection of low-frequency GWs will help answer numerous astrophysical, cosmological, and theoretical questions.

The mission is expected to be launched in 2034. Three spacecraft will trail the Earth around the Sun, in a nearly equilateral triangular configuration with armlengths of about 2.5 million kilometers. Each spacecraft contains two free-falling test masses acting as inertial sensors, with a demonstrated sub-femto- $g$  accuracy [2, 3]. The relative motions of these test masses is measured to picometer precision using laser interferometry. These measurements are then processed on ground to extract GW signals. Each spacecraft carries one ultra-stable oscillator (USO), which provides a unique clock time, used as reference for all systems of the onboard measurement chain. Any timing jitter of the onboard clocks will couple into our interferometric measurements. State-of-the-art space-qualified oscillators typically have an Allan deviation of about  $10^{-13}$  for averaging times above 1 s [4]. This is not sufficient to achieve the picometer test-mass position readout required by LISA.

As a solution, it is planned to perform an independent

measurement of the differential clock jitter [5], which can be used for clock-noise reduction algorithms. A first version of such an algorithm was presented in [6], which perfectly cancels clock noise assuming constant armlengths. In [7], it was shown that this algorithm can be extended to linearly time-varying armlengths and still reduces clock noise below requirements. This correction algorithm is designed to be applied to the so-called time-delay interferometry (TDI) combinations, proposed in [8] to reduce the otherwise overwhelming laser frequency noise. TDI combinations synthesize virtual laser noise-free interferometers of different topologies. Under the assumption of constant armlengths, it has been shown [9] that all topologies can be generated from a finite set of combinations. However, analytic and numerical studies [10–13] have shown that these first-generation combinations are not enough to reach the required laser-noise reduction. Instead, one must use second-generation combinations, for which no finite set of generators has been found [14]. Each of these combinations might be useful for scientific analysis as it possesses a unique response to instrumental noise and gravitational signals. The previously mentioned correction algorithm is only applicable to a specific subset of solutions, namely the Michelson and Sagnac topologies. We present here a general clock-noise reduction algorithm which can be applied to almost any second-generation TDI combination.

In section II, we introduce a model for the phasemeter measurements produced by LISA. Then, in section III, we study how clock noise enters in the standard TDI combinations, and propose a general algorithm to remove it. In section IV, we present numerical simulations, and discuss

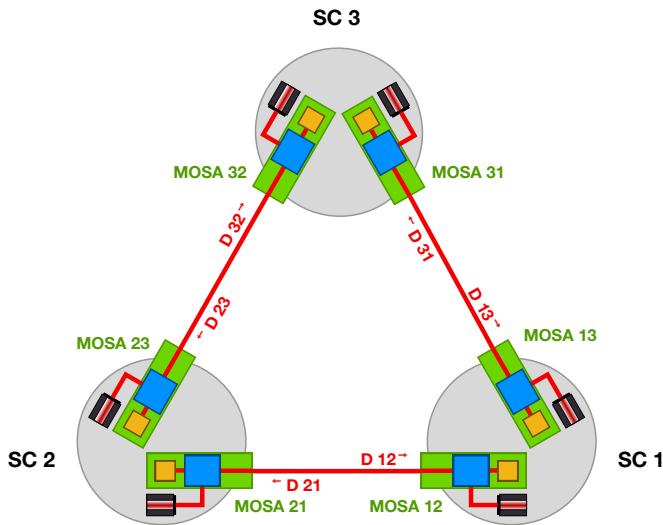


Figure 1. Labelling conventions used for spacecraft, light travel times, lasers, MOSAs, and interferometric measurements.

the main results in section V. In particular, we give models for the limiting effects and compare the performance of our algorithm against existing clock-noise reduction schemes. We conclude in section VI.

## II. PHASEMETER MEASUREMENTS

### A. Description of laser beams

We give here a description of our instrumental model, using the latest recommendations on conventions and notations established by the LISA Consortium (illustrated in fig. 1).

Spacecraft are indexed 1, 2, 3 clockwise when looking down at their solar panels. Any subsystem or measurement uniquely attached to a spacecraft is labelled with the same index. E.g., each spacecraft hosts a single clock.

Movable optical system assemblies (MOSAs) are labelled with two indices  $ij$ . The former matches the index  $i$  of the spacecraft hosting the MOSA, while the second index is that of the spacecraft  $j$  exchanging light with the MOSA. Any subsystem or measurement uniquely attached to a MOSA shares the same indices.

In the following, we make use of two sets of time coordinates. On one hand, the spacecraft proper time  $\tau_i$  is used to describe all physical signals in spacecraft  $i$ . On the other hand, each spacecraft hosts a clock implemented by an USO. Instrumental imperfections of this USO are modeled by the clock timing jitter  $q_i(\tau)$ , measured with respect to the spacecraft proper time. This defines the clock time coordinate

$$\hat{\tau}_i(\tau) = \tau + q_i(\tau). \quad (1)$$

We neglect any deterministic clock imperfections, such as a constant frequency offset, and assume that  $q_i$  can

be modelled as zero-mean Gaussian noise with a power spectral density (PSD) given in eq. (45).

In order to reduce clock noise, we transfer clock tones between the spacecraft. Clock information is imprinted on the laser beams via a phase modulation at GHz frequencies. Because the modulation index is small (around 0.15), we can describe the modulated laser beam as the superposition of three independent beams, each with its own total frequency: the carrier frequency  $\nu_c(\tau)$ , the upper sideband frequency, and the lower sideband frequency. In the following, we assume that the information contained in both sidebands is identical, and will only model the upper sideband, designated simply as *the sideband*. Its total frequency is denoted  $\nu_{\text{sb}}(\tau)$ .

We decompose the carrier and sideband total frequencies into a constant nominal laser frequency  $\nu_0 = 281.6$  THz, large out-of-band offsets  $\nu^o(\tau)$ , and small in-band fluctuations  $\nu^\epsilon(\tau)$ ,

$$\nu_c(\tau) = \nu_0 + \nu_c^o(\tau) + \nu_c^\epsilon(\tau), \quad (2a)$$

$$\nu_{\text{sb}}(\tau) = \nu_0 + \nu_{\text{sb}}^o(\tau) + \nu_{\text{sb}}^\epsilon(\tau). \quad (2b)$$

Frequency offsets contain Doppler shifts [15], the tens-of-MHz programmed offsets as determined by the frequency plan, and constant sideband frequency offsets  $\nu_{ij}^m \approx 2.4$  GHz<sup>1</sup>. Frequency fluctuations are used to model instrumental noise.

In this paper, we assume all six lasers to be independent. On MOSA  $ij$ , the laser source  $ij$  delivers the *local carrier and sideband* with respective frequencies of  $\nu_{ij,c}(\tau)$  and  $\nu_{ij,\text{sb}}(\tau)$ , which we decompose into offsets and fluctuations according to eqs. (2a) and (2b),

$$\nu_{ij,c}^o(\tau) = O_{ij}, \quad (3a)$$

$$\nu_{ij,c}^\epsilon(\tau) = 0, \quad (3b)$$

$$\nu_{ij,\text{sb}}^o(\tau) = O_{ij} + \nu_{ij}^m, \quad (3c)$$

$$\nu_{ij,\text{sb}}^\epsilon(\tau) = \nu_{ij}^m(\dot{q}_i(\tau) + \dot{N}_{ij}^m(\tau)). \quad (3d)$$

We assume here that the programmed frequency offsets  $O_{ij}$  are constant. In addition, we assume that the traditional TDI algorithms sufficiently suppress primary noises (e.g., laser noise or spacecraft jitter) such that we can neglect any noises apart from the clock timing jitter. In addition, we account for any imperfections in the sideband modulation chain, such as errors due to electrical-frequency conversions or optical modulators, by a modulation noise term  $N_{ij}^m(\tau)$ . Both  $N_{ij}^m(\tau)$  and  $\dot{q}_i(\tau)$  are expressed as fractional frequency fluctuations, scaled by the modulation frequency  $\nu_{ij}^m$ .

On MOSA  $ij$ , we call *distant carrier and sideband* the beams received from the distant MOSA  $ji$ . We define

<sup>1</sup> In this paper, we assume that on each spacecraft, the left-handed modulation signals are at exactly 2.4 GHz, while the right-handed ones are at 2.401 GHz.

the delay operator associated with the light travel time<sup>2</sup>  $d_{ij}(\tau)$  between spacecraft  $j$  and  $i$  as

$$\mathbf{D}_{ij}x(\tau) = x(t - d_{ij}(\tau)), \quad (4)$$

for any signal  $x(\tau)$ . Because these light travel times are time-varying, we have to account for Doppler shifts proportional to the time derivatives of the light travel times  $\dot{d}_{ij}(\tau)$  [15]. Therefore, we define the Doppler-delay operator,

$$\dot{\mathbf{D}}_{ij}x(\tau) = (1 - \dot{d}_{ij}(\tau))x(t - d_{ij}(\tau)). \quad (5)$$

Onboard MOSA  $ij$ , the distant carrier and sideband are then given by

$$\nu_{ij \leftarrow j, c}(\tau) = \dot{\mathbf{D}}_{ij}\nu_{ji, c}(\tau), \quad (6a)$$

$$\nu_{ij \leftarrow j, sb}(\tau) = \dot{\mathbf{D}}_{ij}\nu_{ji, sb}(\tau). \quad (6b)$$

We decompose again these frequencies into offsets and fluctuations. Using eqs. (2a), (2b) and (3a) to (3d), we have

$$\nu_{ij \leftarrow j, c}^o(\tau) = \dot{\mathbf{D}}_{ij}O_{ji} - \nu_0\dot{d}_{ij}(\tau), \quad (7a)$$

$$\nu_{ij \leftarrow j, c}^\epsilon(\tau) = 0, \quad (7b)$$

$$\nu_{ij \leftarrow j, sb}^o(\tau) = \dot{\mathbf{D}}_{ij}(O_{ji} + \nu_{ji}^m) - \nu_0\dot{d}_{ij}(\tau), \quad (7c)$$

$$\nu_{ij \leftarrow j, sb}^\epsilon(\tau) = \nu_{ji}^m\dot{\mathbf{D}}_{ij}(\dot{q}_j(\tau) + \dot{N}_{ji}^m(\tau)). \quad (7d)$$

Local laser beams are also exchanged with adjacent MOSAs. On MOSA  $ij$ , we call the beams received from adjacent MOSA  $ik$  the *adjacent carrier and sideband*. We ignore any effect due to the propagation of the beams inside a spacecraft, such that their frequencies decomposed into offsets and fluctuations are simply given as

$$\nu_{ij \leftarrow ik, c}^o(\tau) = O_{ik}, \quad (8a)$$

$$\nu_{ij \leftarrow ik, c}^\epsilon(\tau) = 0, \quad (8b)$$

$$\nu_{ij \leftarrow ik, sb}^o(\tau) = O_{ik} + \nu_{ik}^m, \quad (8c)$$

$$\nu_{ij \leftarrow ik, sb}^\epsilon(\tau) = \nu_{ik}^m(\dot{q}_i(\tau) + \dot{N}_{ik}^m(\tau)). \quad (8d)$$

## B. Interferometric measurements

Onboard each MOSA, three heterodyne interferometers measure beatnotes frequencies  $\nu_{\text{BN}}(\tau)$ . The photodetectors recording these beatnotes have a limited bandwidth between 5 MHz and 25 MHz, such that only three beatnotes are detected in each interferometer: one between the two carriers of the incoming beams, one between the upper sidebands and one between the

lower sidebands. We give here only expressions for the carrier-carrier  $\nu_{\text{BN}, c}(\tau)$  and upper sideband-upper sideband  $\nu_{\text{BN}, sb}(\tau)$  beatnotes.

Following the formalism introduced in eqs. (2a) and (2b), we decompose the beatnote frequencies into large out-of-band offsets and small in-band fluctuations,  $\nu_{\text{BN}}(\tau) = \nu_{\text{BN}}^o(\tau) + \nu_{\text{BN}}^\epsilon(\tau)$ . If we denote the two incoming beams 1 and 2, we have

$$\nu_{\text{BN}, c}^o(\tau) = \nu_{1, c}^o(\tau) - \nu_{2, c}^o(\tau), \quad (9a)$$

$$\nu_{\text{BN}, c}^\epsilon(\tau) = \nu_{1, c}^\epsilon(\tau) - \nu_{2, c}^\epsilon(\tau), \quad (9b)$$

$$\nu_{\text{BN}, sb}^o(\tau) = \nu_{1, sb}^o(\tau) - \nu_{2, sb}^o(\tau), \quad (9c)$$

$$\nu_{\text{BN}, sb}^\epsilon(\tau) = \nu_{1, sb}^\epsilon(\tau) - \nu_{2, sb}^\epsilon(\tau). \quad (9d)$$

The *inter-spacecraft (ISC) interferometer* mixes the local and distant beams. Using eqs. (3a) to (3d) and eqs. (7a) to (7d), we find

$$\nu_{\text{isc}, ij, c}^o(\tau) = \dot{\mathbf{D}}_{ij}O_{ji} - O_{ij} - \nu_0\dot{d}_{ij}(\tau), \quad (10a)$$

$$\nu_{\text{isc}, ij, c}^\epsilon(\tau) = 0, \quad (10b)$$

$$\nu_{\text{isc}, ij, sb}^o(\tau) = (\dot{\mathbf{D}}_{ij}O_{ji} - O_{ij} - \nu_0\dot{d}_{ij}(\tau)) + (\dot{\mathbf{D}}_{ij}\nu_{ji}^m - \nu_{ij}^m), \quad (10c)$$

$$\nu_{\text{isc}, ij, sb}^\epsilon(\tau) = \nu_{ji}^m\dot{\mathbf{D}}_{ij}(\dot{q}_j(\tau) + \dot{N}_{ji}^m(\tau)) - \nu_{ij}^m(\dot{q}_i(\tau) + \dot{N}_{ij}^m(\tau)). \quad (10d)$$

The *reference (REF) interferometer* mixes the local and adjacent beams. Using eqs. (3a) to (3d) and eqs. (8a) to (8d),

$$\nu_{\text{ref}, ij, c}^o(\tau) = O_{ik} - O_{ij}, \quad (11a)$$

$$\nu_{\text{ref}, ij, c}^\epsilon(\tau) = 0, \quad (11b)$$

$$\nu_{\text{ref}, ij, sb}^o(\tau) = (O_{ik} - O_{ij}) + (\nu_{ik}^m - \nu_{ij}^m), \quad (11c)$$

$$\nu_{\text{ref}, ij, sb}^\epsilon(\tau) = \nu_{ik}^m(\dot{q}_i(\tau) + \dot{N}_{ik}^m(\tau)) - \nu_{ij}^m(\dot{q}_i(\tau) + \dot{N}_{ij}^m(\tau)). \quad (11d)$$

The *test-mass (TM) interferometer* also mixes the local and adjacent beams, and differs from the REF interferometer only because the local beam is reflected off the TM. Since we neglect any propagation inside the spacecraft, we simply have  $\nu_{\text{tm}, ij} = \nu_{\text{ref}, ij}$ .

## C. Measurement sampling

The analog beatnotes are sampled, digitized and time-stamped by the phasemeter, which uses a signal derived from the local USO as timing reference [5]. Therefore, all samples have timestamps attached that are equally sampled with respect to the local clock.

Formally, we need to express the signals we wish to sample as functions of the onboard clock times. For an analog signal  $s(\tau)$  expressed in phase and as a function of the proper time, the same signal sampled to the clock time reads

$$\tilde{s}(\tau) = s(\tau_i(\tau)), \quad (12)$$

<sup>2</sup> In all generality, delay operators must include the conversion between the emitting and receiving spacecraft proper time coordinates. We include these corrections based on a derivation provided by the SYRTE ‘‘Theory and Metrology’’ group.

where  $\tau_i(\tau)$  is the spacecraft proper time at which the onboard clock shows  $\tau$ . Here,  $\tau_i(\tau)$  can be computed by inverting eq. (1). At first order in  $q_i$ , we have

$$\tau_i(\tau) \approx \tau - q_i(\tau). \quad (13)$$

Using this result, we find at first order in  $q_i$ ,

$$\tilde{s}(\tau) \approx s(\tau) - \dot{s}(\tau)q_i(\tau), \quad (14)$$

which we can differentiate to obtain, in frequency,

$$\begin{aligned} \frac{d\tilde{s}}{d\tau}(\tau) &\approx (1 - \dot{q}_i(\tau))\dot{s}(\tau) - \ddot{s}(\tau)q_i(\tau) \\ &\approx (1 - \dot{q}_i(\tau))\dot{s}(\tau), \end{aligned} \quad (15)$$

where we neglect the term  $\ddot{s}(\tau)q_i(\tau)$  since the total beatnote frequencies are evolving very slowly ( $\ddot{s}(\tau) \approx 10^2 \text{ Hz s}^{-1}$ ) [15].

Decomposing  $\dot{s}(\tau)$  into frequency offsets  $\dot{s}^o(\tau)$  and fluctuations  $\dot{s}^\epsilon(\tau)$ , and neglecting second-order terms in  $\dot{q}_i(\tau)\dot{s}^\epsilon(\tau)$ , eq. (15) becomes

$$\frac{d\tilde{s}}{d\tau}(\tau) \approx \dot{s}^o(\tau) - \dot{q}_i(\tau)\dot{s}^o(\tau) + \dot{s}^\epsilon(\tau). \quad (16)$$

We can now decompose again the resulting sampled signal into offsets and fluctuations,

$$\frac{d\tilde{s}^o}{d\tau}(\tau) \approx \dot{s}^o(\tau), \quad (17a)$$

$$\frac{d\tilde{s}^\epsilon}{d\tau}(\tau) \approx \dot{s}^\epsilon(\tau) - \dot{q}_i(\tau)\dot{s}^o(\tau). \quad (17b)$$

#### D. Measurement equations

We saw in the previous section that clock noise only affects frequency fluctuations. Let us write the sampled beatnote frequency fluctuations from their analog descriptions given in the previous section. For concision, we will drop the tilde and denote  $\text{isc}_{ij}(\tau)$ ,  $\text{ref}_{ij}(\tau)$ , and  $\text{tm}_{ij}(\tau)$  the sampled ISC, REF, and TM beatnote frequency fluctuations, respectively. In addition, we will drop the explicit time dependency of all variables for the sake of readability, and introduce shortened notations for the time-varying beatnote frequency offsets,

$$a_{ij} = \nu_{\text{isc}_{ij},c}^o \quad \text{and} \quad b_{ij} = \nu_{\text{ref}_{ij},c}^o. \quad (18)$$

Plugging eqs. (10b) and (10d) in eq. (17b) yields

$$\text{isc}_{ij,c} = -\dot{q}_i a_{ij}, \quad (19a)$$

$$\begin{aligned} \text{isc}_{ij,cb} &= \nu_{ji}^m \dot{\mathbf{D}}_{ij}(\dot{q}_j + \dot{N}_{ji}^m) - \nu_{ij}^m(\dot{q}_i + \dot{N}_{ij}^m) \\ &\quad - \dot{q}_i(a_{ij} + \dot{\mathbf{D}}_{ij}\nu_{ji}^m - \nu_{ij}^m). \end{aligned} \quad (19b)$$

Similarly, using eqs. (11b) and (11d) gives

$$\text{ref}_{ij,c} = -\dot{q}_i b_{ij}, \quad (20a)$$

$$\begin{aligned} \text{ref}_{ij,cb} &= \nu_{ik}^m(\dot{q}_i + \dot{N}_{ik}^m) - \nu_{ij}^m(\dot{q}_j + \dot{N}_{ij}^m) \\ &\quad - \dot{q}_i(b_{ij} + \nu_{ik}^m - \nu_{ij}^m). \end{aligned} \quad (20b)$$

As discussed in section II B, TM beatnote frequency fluctuations are identical to the REF ones.

### III. CLOCK-NOISE REDUCTION

#### A. Detrending

In reality, only the total beatnote frequencies (e.g., the total ISC carrier-carrier beatnote frequency  $a_{ij} + \text{isc}_{ij,c}$ ) are directly measured by the phasemeter and telemetered to Earth. The current baseline for LISA data processing is to filter out-of-band offsets from the total frequencies to recover the previously described in-band frequency fluctuations ( $\text{isc}_{ij,c}$  in the previous example).

In the following, we assume that this process can be achieved without errors, and will use the beatnote frequency fluctuations described in section II D.

#### B. Intermediary variables

The so-called TDI intermediary variables  $\xi$  are constructed to remove spacecraft jitter noise [16],

$$\xi_{ij} = \text{isc}_{ij,c} + \frac{(\text{ref}_{ij,c} - \text{tm}_{ij,c})}{2} + \dot{\mathbf{D}}_{ij} \frac{(\text{ref}_{ji,c} - \text{tm}_{ji,c})}{2}. \quad (21a)$$

Next up, the  $\eta$  intermediary variables remove half of the laser noise, respectively. They read [16],

$$\eta_{ij} = \xi_{ij} + \dot{\mathbf{D}}_{ij} \frac{\text{ref}_{ji,c} - \text{ref}_{jk,c}}{2}, \quad (22a)$$

$$\eta_{ik} = \xi_{ik} + \frac{\text{ref}_{ij,c} - \text{ref}_{ik,c}}{2}, \quad (22b)$$

for left  $ij$  and right  $ik$  MOSAs, respectively.

Inserting eqs. (19a) and (20a) in these expressions, we find how clock noise enters these intermediary variables,

$$\eta_{ij} = \dot{\mathbf{D}}_{ij} b_{jk} \dot{q}_j - a_{ij} \dot{q}_i, \quad (23)$$

$$\eta_{ik} = -(b_{ij} + a_{ik}) \dot{q}_i. \quad (24)$$

Note that  $b_{ij} = -b_{ik}$ . In the following, we choose to only use reference beatnote frequencies  $b_{ij}$  from left MOSAs.

#### C. Clock-noise residuals

From these intermediary variables, we can build laser noise-free TDI combinations. They can be expressed as polynomials of delay operators  $\mathbf{P}_{ij}$ , in the form

$$\text{TDI} = \sum_{i,j \in \mathcal{I}_2} \mathbf{P}_{ij} \eta_{ij}. \quad (25)$$

where  $\mathcal{I}_2 = \{(1, 2), (2, 3), (3, 1), (1, 3), (3, 2), (2, 1)\}$  is the set of the 6 MOSA index pairs.

Inserting eqs. (23) and (24), we find that clock noise enters in the TDI combination as

$$\text{TDI}^q = \sum_{i,j,k \in \mathcal{I}_3^+} [\mathbf{P}_{ki} \dot{\mathbf{D}}_{ki} - \mathbf{P}_{ik}] b_{ij} \dot{q}_i - \sum_{i,j \in \mathcal{I}_2} \mathbf{P}_{ij} a_{ij} \dot{q}_i, \quad (26)$$

with  $\mathcal{I}_3^+ = \{(1, 2, 3), (2, 3, 1), (3, 1, 2)\}$  as the set of triplets of spacecraft indices in ascending order.

To estimate the contribution of clock noise before any correction, we assume that all light travel times are constant and equal to  $L$ , such that we can commute delay operators. As shown in [12], these commutators only yield multiplicative terms  $\ll 1$ . Also, we suppose that all clock noises are uncorrelated but have the same PSD  $S_{\dot{q}}(\omega)$ . Lastly, we assume that beatnote frequency offsets are constant. The clock noise residual PSD then reads

$$S_{\text{TDI}^q}(\omega) \approx \sum_{i,j,k \in \mathcal{I}_3^+} \left| a_{ij} \tilde{\mathbf{P}}_{ij}(\omega) + a_{ji} \tilde{\mathbf{P}}_{ji}(\omega) - b_{ij} [\tilde{\mathbf{P}}_{ik}(\omega) - \tilde{\mathbf{P}}_{ki}(\omega) \tilde{\mathbf{D}}_{ki}(\omega)] \right|^2 S_{\dot{q}}(\omega), \quad (27)$$

Here,  $\tilde{\mathbf{D}}_{ij}$  and  $\tilde{\mathbf{P}}_{ij}$  are the Fourier transforms of delay operators and polynomials thereof, see [12] for further information.

As an example, we can use eq. (27) to work out clock noise residuals in the second-generation Michelson combination  $X_2$ , as defined in [16],

$$X_2 = (1 - \dot{\mathbf{D}}_{121} - \dot{\mathbf{D}}_{12131} + \dot{\mathbf{D}}_{1312121})(\eta_{13} + \dot{\mathbf{D}}_{13}\eta_{31}) - (1 - \dot{\mathbf{D}}_{131} - \dot{\mathbf{D}}_{13121} + \dot{\mathbf{D}}_{1213131})(\eta_{12} + \dot{\mathbf{D}}_{12}\eta_{21}). \quad (28)$$

We find that

$$S_{X_2^q}(\omega) \approx 16 \sin^2(2\omega L) \sin^2(\omega L) A_{X_2}(\omega) S_{\dot{q}}(\omega), \quad (29)$$

with  $A_{X_2}(\omega)$  is a scaling factor that depends only on the beatnote frequencies,

$$A_{X_2}(\omega) = (a_{12} - a_{13})^2 + a_{21}^2 + a_{31}^2 - 4b_{12}(a_{12} - a_{13} - b_{12}) \sin^2(\omega L). \quad (30)$$

Figure 2 shows this clock noise residual for a state-of-the-art space-qualified USO with  $S_{\dot{q}}(f) = 4 \times 10^{-27} f^{-1}$  in fractional frequency fluctuations [17], and a realistic set of beatnote frequency offsets. We compared it to a typical 1 pm LISA noise allocation for a single noise source,

$$S_{X_2^{\text{alloc}}}(\omega) = 64\omega^2 \sin^2(\omega L) \sin^2(2\omega L) \times \left( \frac{1 \text{ pmHz}^{-1/2}}{\lambda} \right)^2 \left[ 1 + \left( \frac{2 \times 10^{-3} \text{ Hz}}{\omega/2\pi} \right)^4 \right]. \quad (31)$$

We see that below 0.2 Hz, clock noise violates this requirement and must be suppressed.

#### D. Building correcting expression

Inspecting eq. (26), we observe that clock noise enters in our TDI combination coupled with delay polynomials.

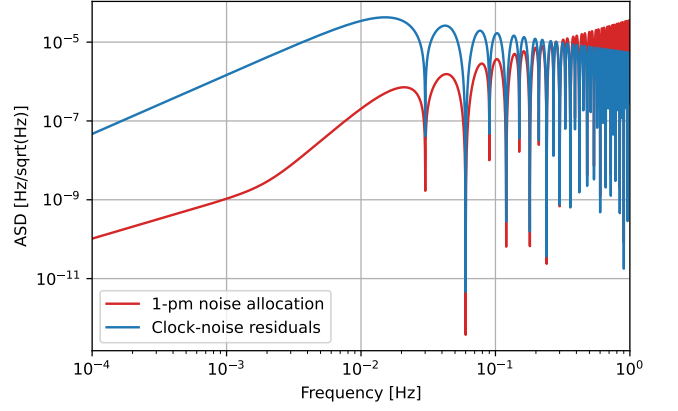


Figure 2. Comparison of the residual clock noise in second-generation Michelson  $X_2$  combination, and the usual LISA 1 pm noise allocation curve. We assumed here a state-of-the-art space-qualified USO and a realistic set of beatnote frequency offsets.

We can rearrange it to get

$$\begin{aligned} \text{TDI}^q &= \sum_{i,j,k \in \mathcal{I}_3^+} \mathbf{P}_{ij}(b_{jk} - a_{ij})\dot{q}_i \\ &\quad - \mathbf{P}_{ik}(b_{ij} + a_{ik})\dot{q}_i \\ &\quad + \mathbf{P}_{ij}(\dot{\mathbf{D}}_{ij}b_{jk}\dot{q}_j - b_{jk}\dot{q}_i). \end{aligned} \quad (32)$$

In the previous equations, beatnote frequency offsets  $a_{ij}$ ,  $b_{ij}$  are time-dependent, c.f. eq. (10a). As such, commuting them with a delay operator yields an error term. This effect will be studied in section V A. In this section, we neglect it and write the previous equation as

$$\begin{aligned} \text{TDI}^q &\approx \sum_{i,j,k \in \mathcal{I}_3^+} (b_{jk} - a_{ij})\mathbf{P}_{ij}\dot{q}_i \\ &\quad - (b_{ij} + a_{ik})\mathbf{P}_{ik}\dot{q}_i \\ &\quad + b_{jk}\mathbf{P}_{ij}(\dot{\mathbf{D}}_{ij}\dot{q}_j - \dot{q}_i). \end{aligned} \quad (33)$$

We observe that clock noise appears on the right side of the  $\mathbf{P}_{ij}$ , either *directly* as  $\dot{q}_i$ , or as a *differential term*  $\dot{\mathbf{D}}_{ij}\dot{q}_j - \dot{q}_i$ .

We will now see that the sideband-sideband beatnotes introduced in section IIB can provide a direct measurement of the differential clock noise. We form the dimensionless quantity

$$r_{ij} = \frac{\text{isc}_{ij,\text{sb}} - \text{isc}_{ij,\text{c}}}{\nu_{ji}^m}. \quad (34)$$

By inserting eqs. (19a) and (19b) into the previous expression, we see that  $r_{ij}$  directly measures the differential clock noise appearing in eq. (32),

$$r_{ij} = \dot{\mathbf{D}}_{ij}\dot{q}_j - \dot{q}_i, \quad (35)$$

where we neglect the modulation noise for now. The effect of modulation noise and an additional processing step for its partial mitigation are discussed in section V B.

Because the beatnote frequency offsets are measured and the delay polynomials are known, we can subtract  $\sum_{i,j,k \in \mathcal{I}_3^+} b_{jk} \mathbf{P}_{ij} r_{ij}$  from our TDI combination to remove the last term of eq. (32).

We are left with the first two terms in the sum in eq. (32). Vallisneri discusses in [18] how any arbitrary interferometer can be synthesized out of a set of 6 one-way interferometric measurements  $y_{ij}$  between the LISA spacecraft. The  $r_{ij}$  are of exactly the same form as the  $y_{ij}$  used in [18], just expressed in terms of clock noise instead of laser noise. Therefore, we can apply the same algorithm<sup>3</sup> to construct any expression of the form  $(\dot{\mathbf{D}}_{i_1, i_2, \dots, i_n} q_{i_n} - q_{i_1})$  from the  $r_{ij}$ .

Each delay polynomial  $\mathbf{P}_{ij}$  in eq. (25) is the sum of  $n_{ij}$  chained delay operators with signs  $\sigma_{ij}^k$ . It can be written as

$$\mathbf{P}_{ij} = \sum_{k=1}^{n_{ij}} \sigma_{ij}^k \dot{\mathbf{D}}_{A_{ij}^k, \dots, B_{ij}^k}, \quad (36)$$

where we denote the first and last indices of the chained delay operators in the  $k$ -th summand with  $A_{ij}^k$  and  $B_{ij}^k$ , respectively. By design of the TDI algorithm, we always have  $B_{ij}^k = i$ .

Using Vallisneri's algorithm for each summand, we can construct

$$R_{ij} = \sum_{k=1}^{n_{ij}} \sigma_{ij}^k \left( \dot{\mathbf{D}}_{A_{ij}^k, \dots, i} \dot{q}_i - \dot{q}_{A_{ij}^k} \right). \quad (37)$$

We have

$$\mathbf{P}_{ij} \dot{q}_i - R_{ij} = \sum_{k=1}^{n_{ij}} \sigma_{ij}^k \dot{q}_{A_{ij}^k}. \quad (38)$$

In most second generation TDI combinations<sup>4</sup>, this last term is vanishing, such that we have  $R_{ij} = P_{ij} q_i$ . Therefore, we can subtract them from eq. (32) to remove the last clock-noise terms.

In the special case where one summand in  $\mathbf{P}_{ij}$ , say the  $n$ -th term, does not contain any delay, we skip it in the construction of  $R_{ij}$  (eq. (37)). An extra term  $\sigma_{ij}^n \dot{q}_i$  is to be accounted for in eq. (38), which has to cancel with one of the  $\sigma_{ij}^k \dot{q}_{A_{ij}^k}$ .

The full corrected TDI combination therefore reads

$$\begin{aligned} \text{TDI}^c = \text{TDI} - \sum_{i,j,k \in \mathcal{I}_3^+} (b_{jk} - a_{ij}) R_{ij} \\ - (b_{ij} + a_{ik}) R_{ik} \\ + b_{jk} \mathbf{P}_{ij} r_{ij}. \end{aligned} \quad (39)$$

<sup>3</sup> Note that [18] uses a different notation. We translated their algorithm to our notation in appendix A.

<sup>4</sup> We explicitly tested it for all second generation TDI combinations up to 16 links presented in [13]. We conjecture that it is valid for any second generation variable derived from geometric principles.

Note that this algorithm can be applied without modification to TDI variables containing not only delays, but also advancements [13, 18].

### E. Example: correcting clock noise for $X_2$

As an example, we apply our algorithm to the second-generation Michelson combination  $X_2$  given in eq. (28). Following the decomposition of eq. (25),

$$\mathbf{P}_{12} = -(1 - \dot{\mathbf{D}}_{131} - \dot{\mathbf{D}}_{13121} + \dot{\mathbf{D}}_{1213131}), \quad (40a)$$

$$\mathbf{P}_{23} = 0, \quad (40b)$$

$$\mathbf{P}_{31} = (1 - \dot{\mathbf{D}}_{121} - \dot{\mathbf{D}}_{12131} + \dot{\mathbf{D}}_{1312121}) \dot{\mathbf{D}}_{13}, \quad (40c)$$

$$\mathbf{P}_{21} = -(1 - \dot{\mathbf{D}}_{131} - \dot{\mathbf{D}}_{13121} + \dot{\mathbf{D}}_{1213131}) \dot{\mathbf{D}}_{12}, \quad (40d)$$

$$\mathbf{P}_{32} = 0, \quad (40e)$$

$$\mathbf{P}_{13} = (1 - \dot{\mathbf{D}}_{121} - \dot{\mathbf{D}}_{12131} + \dot{\mathbf{D}}_{1312121}). \quad (40f)$$

Applying Vallisneri's algorithm, we construct the  $R_{ij}$  variables verifying eq. (37). They read

$$\begin{aligned} R_{12} = -(1 - \dot{\mathbf{D}}_{131})(r_{12} + \dot{\mathbf{D}}_{12} r_{21}) \\ + (2 - \dot{\mathbf{D}}_{121} - \dot{\mathbf{D}}_{12131})(r_{13} + \dot{\mathbf{D}}_{13} r_{31}), \end{aligned} \quad (41a)$$

$$R_{23} = 0, \quad (41b)$$

$$\begin{aligned} R_{31} = -(2 - \dot{\mathbf{D}}_{131} - \dot{\mathbf{D}}_{13121})(r_{12} + \dot{\mathbf{D}}_{12} r_{21}) \\ + (1 - \dot{\mathbf{D}}_{121})(r_{13} + \dot{\mathbf{D}}_{13} r_{31}) \end{aligned} \quad (41c)$$

$$+ (1 - \dot{\mathbf{D}}_{121} - \dot{\mathbf{D}}_{12131} + \dot{\mathbf{D}}_{1312121}) r_{13},$$

$$\begin{aligned} R_{21} = -(1 - \dot{\mathbf{D}}_{131})(r_{12} + \dot{\mathbf{D}}_{12} r_{21}) \\ - (1 - \dot{\mathbf{D}}_{131} - \dot{\mathbf{D}}_{13121} + \dot{\mathbf{D}}_{1213131}) r_{12} \end{aligned} \quad (41d)$$

$$+ (2 - \dot{\mathbf{D}}_{121} - \dot{\mathbf{D}}_{12131})(r_{13} + \dot{\mathbf{D}}_{13} r_{31}),$$

$$R_{32} = 0, \quad (41e)$$

$$\begin{aligned} R_{13} = -(2 - \dot{\mathbf{D}}_{131} - \dot{\mathbf{D}}_{13121})(r_{12} + \dot{\mathbf{D}}_{12} r_{21}) \\ + (1 - \dot{\mathbf{D}}_{121})(r_{13} + \dot{\mathbf{D}}_{13} r_{31}). \end{aligned} \quad (41f)$$

These can be directly inserted into eq. (39) to get the corrected variable  $X_2^c$ .

## IV. NUMERICAL SIMULATIONS

To complement the theoretical studies presented above, we conducted numerical experiments to verify the clock-noise suppression capabilities of this algorithm. We simulated the signals presented in section IIB using the Python tool LISA Instrument, which is based on the official LISA Consortium simulator LISANode [19]. We then used the Python tool PyTDI to generate the second-generation Michelson TDI data streams  $X_2$ , as well as the corresponding clock correction, all described in section III.

Laser beams and interferometric measurements are simulated in frequency. In addition, we use the decomposition in frequency offsets and fluctuations presented

in section II A. Each of these variables is represented by a 64-bit floating-point number (double precision), such that they have sufficient dynamic range not to be limited by quantization noise. Note that in reality, we will only have access to the sum of these two variables, and need to decompose them on-ground before we can apply this clock-correction algorithm (c.f. section III A).

In order not to be limited by other numerical effects, such as interpolation errors or flexing-filtering couplings [12], we use an unrealistically high sampling rate of 10 Hz for the full simulation chain. By doing so, we omit any simulation of on-board filters. The duration of our simulation is set to  $10^6$  s, i.e.,  $10^7$  samples.

The propagation of laser beams between spacecraft is implemented using Lagrange fractional delay filters of order 31. Given our high sampling rate, they do not cause any observable artifact in our frequency band of interest and remain computationally tractable. Light travel times and their derivatives are computed from realistic orbits provided by ESA. These light travel times include relativistic corrections up to terms in  $1/c$ , including the Sagnac effect and the Shapiro delay.

We use the following programmed offsets, see eq. (3a),

$$O_{12} = 8.1 \text{ MHz}, \quad O_{21} = -9.5 \text{ MHz}, \quad (42)$$

$$O_{13} = 1.4 \text{ MHz}, \quad O_{31} = 10.3 \text{ MHz}, \quad (43)$$

$$O_{23} = 9.2 \text{ MHz}, \quad O_{32} = -11.6 \text{ MHz}. \quad (44)$$

Our simulated clock noise matches that of a state-of-the-art space-qualified USO with

$$S_{\dot{q}}(f) = 4 \times 10^{-27} f^{-1} \quad (45)$$

in fractional frequency deviations, generated using a variant of the infinite RC model [20]. We do not simulate any deterministic clock errors, such as constant timing and frequency offsets or higher order frequency drifts due to aging of the oscillators.

Modulation errors are based on a fit of the 2 W-fiber amplifier (red) curve from figure 5.13 in [5]. In fractional frequency deviations with respect to the modulation frequency, they are given by

$$S_{\dot{N}_m}(f) = 5.2 \times 10^{-14} f^{1/3}. \quad (46)$$

Note that this noise level does not meet the requirements for LISA [5], and consequently also violates our 1 pm-noise allocation curve. Laser development is ongoing to achieve the required noise levels in line with the stringent timing requirements<sup>5</sup>.

Because of LISA's frequency distribution system design [5], only one of the two modulation signals on a spacecraft has a direct low-noise relationship to the pilot tone used as timing reference. Therefore, to demonstrate the correctness of our algorithm, we make the working

assumption that the right hand-side modulation noises (indexed 13, 32, 21) are 10 times higher, i.e. with a spectrum

$$S_{\dot{N}_m}(f) = 5.2 \times 10^{-13} f^{1/3}. \quad (47)$$

To compute our TDI combinations, we also use order-31 Lagrange fractional delay filters.

Figure 3 presents the results of our numerical experiments. We used Welch method to estimate the spectra, with segments of 200 000 samples and a *Nuttall* window function. As a reference, we also plot in red the usual LISA Performance Model's 1 pm-noise allocation curve, given by eq. (31).

The blue and green curves represent the amplitude spectral densities (ASDs) of the uncorrected  $X_2$  and corrected  $X_2^c$  second-generation Michelson TDI combinations, in the sole presence of clock noise (we disabled modulation errors). The black dashed line overlaying the former curve represents the theoretical clock-noise content in  $X_2$  from eq. (29). The black dashed line overlaying the green curve, representing our model of the residual clock noise after correction, is discussed in details in section V A and given by eq. (54).

The orange curve represents the modulation errors in the corrected  $X_2^c$  combination. We obtain it by enabling modulation errors in addition to clock noise in the previous simulation. In addition, we perform an additional processing step to remove the higher right hand-side modulation noise terms, see section V B. The overlaid black dashed line shows our analytical expectations, also described in the same section.

## V. DISCUSSION

We see in fig. 3 that our clock-noise reduction algorithm works as expected and that clock noise is reduced to below the noise allocation curve. In addition, our analytical models match perfectly with simulated results.

We discuss in the following paragraphs the models for the residual clock noise after correction, the imperfections in the sideband measurements used for the correction, and other limiting effects that may appear with different simulation parameters but were not visible in our setup. Finally, we compare our algorithm with the previously proposed solution [7].

### A. Time-varying beatnote frequencies

The residual clock noise after correction is dominated by the effect of time-varying beatnote frequencies, which we neglected when deriving the correction. To evaluate this clock-noise residuals, we take the difference between eq. (32) and eq. (33). One gets

$$\text{TDI}^\nu = \sum_{i,j,k \in \mathcal{I}_3^+} ([a_{ij}, \mathbf{P}_{ij}] + [a_{ik}, \mathbf{P}_{ik}]) q_i, \quad (48)$$

<sup>5</sup> M. Hewitson, private communication, (April 9, 2021).

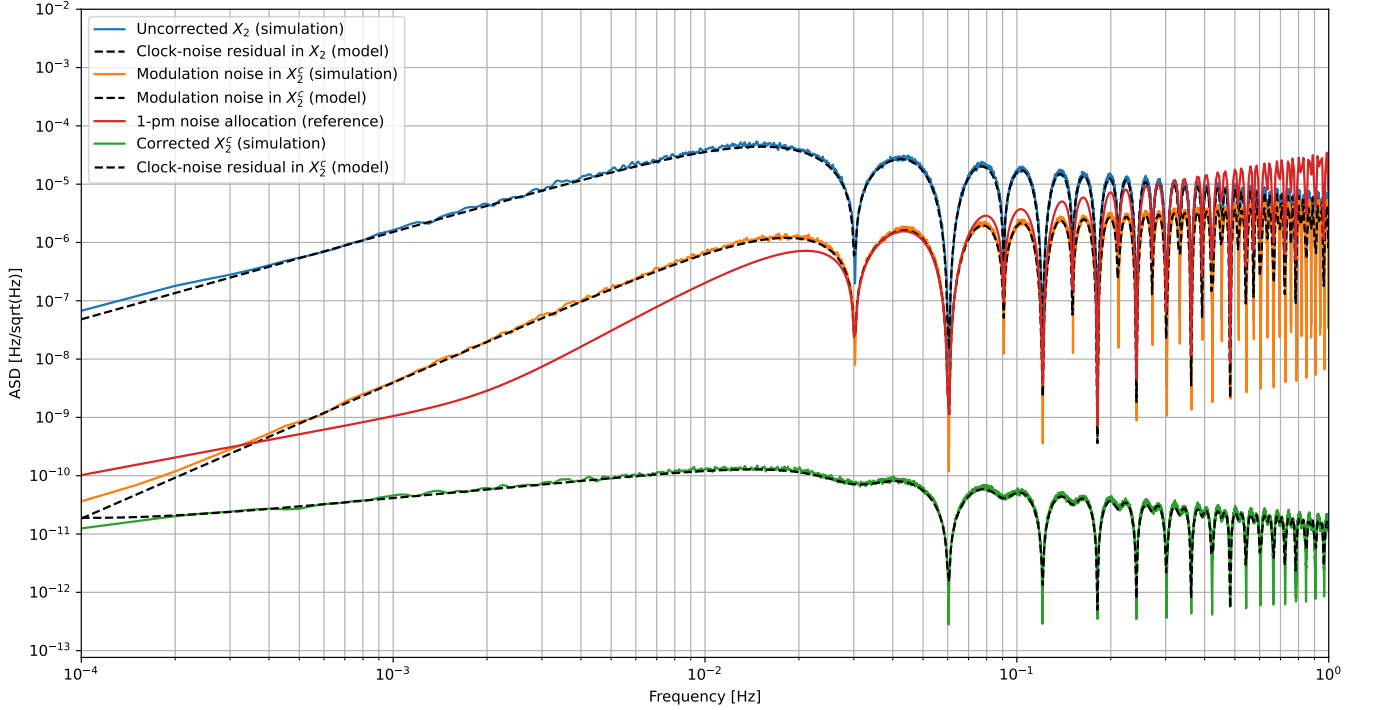


Figure 3. Simulation results. Blue and green curves represent the uncorrected  $X_2$  and corrected  $X_2^c$  combinations in the sole presence of clock noise. The yellow curve shows the level of modulation noise in the corrected variable. Overlaid dashed black lines show our analytical expectations for these quantities. The usual 1 pm-noise allocation curve is shown in red as a reference.

where we used that the reference beatnote offsets are constants in our setup, see eq. (11a), and hence can be freely commuted with delays. Here,  $[A, B] = AB - BA$  stands for the commutator of  $A$  and  $B$ .

We can now assume that all delays are equal and constant, such that a delay operator of  $N$  delays can be written as  $\mathbf{D}^N$ . We can write the delay polynomial  $\mathbf{P}_{ij}$  as

$$\mathbf{P}_{ij} = \sum_{\alpha} \lambda_{\alpha} \mathbf{D}^{N_{\alpha}}, \quad (49)$$

with  $\lambda_{\alpha}$  the factor in front of the term  $\alpha$ , and  $N_{\alpha}$  the number of delays associated with the same term. We now have

$$[a_{ij}, \mathbf{P}_{ij}] = \sum_{\alpha} \lambda_{\alpha} [a_{ij}, \mathbf{D}^{N_{\alpha}}], \quad (50)$$

and similarly for  $\mathbf{P}_{ik}$ .

Let us study one commutator  $[a_{ij}, \mathbf{D}^N]$ . This is an operator, which will be applied on  $q_i$ . Assuming that  $a_{ij}$  is a linear function of time, we can write

$$\begin{aligned} [a_{ij}, \mathbf{D}^N] &= a_{ij}(t)\mathbf{D}^N - (\mathbf{D}^N a_{ij})\mathbf{D}^N \\ &= (a_{ij} - \mathbf{D}^N a_{ij})\mathbf{D}^N \\ &= Nd\dot{a}_{ij}\mathbf{D}^N, \end{aligned}$$

where  $Nd\dot{a}_{ij}$  is a constant. We can then go to the frequency domain to write it as

$$Nd\dot{a}_{ij}e^{-j\omega Nd}. \quad (51)$$

We can therefore define

$$Q_{ij}(\omega) = \sum_{\alpha} \lambda_{\alpha} N_{\alpha} d e^{-j\omega d N_{\alpha}}, \quad (52)$$

such that, still in the frequency domain,

$$[a_{ij}, \mathbf{P}_{ij}] = Q_{ij}\dot{a}_{ij}. \quad (53)$$

Finally, using that clocks are independent but share the same statistical properties, we obtain the following residual from the time-varying beatnote offsets,

$$S_{\text{TDI}^{\nu}}(\omega) = S_q(\omega) \sum_{i,j,k \in \mathcal{I}_3^+} |Q_{ij}(\omega)\dot{a}_{ij} + Q_{ik}(\omega)\dot{a}_{ik}|^2. \quad (54)$$

In our simulation, the average value of the beatnote derivatives evaluate to

$$\dot{a}_{12} \approx \dot{a}_{21} \approx -2.0 \text{ Hz s}^{-1}, \quad (55)$$

$$\dot{a}_{13} \approx \dot{a}_{31} \approx 320 \text{ mHz s}^{-1}, \quad (56)$$

$$\dot{a}_{23} \approx \dot{a}_{32} \approx -58 \text{ mHz s}^{-1}, \quad (57)$$

while their average second derivatives are of the order of, or below,  $10^{-7} \text{ Hz s}^{-2}$ , which is small enough to neglect it in our model. This is also verified by the perfect agreement between model and simulation in fig. 3.



## B. Modulation errors

In section II A, we introduce modulation errors to model imperfections of the sideband modulation. By inserting eqs. (19a) and (19b) into eq. (34), we see that they appear in  $r_{ij}$  as

$$r_{ij} = \frac{\nu_{ji}^m \dot{\mathbf{D}}_{ij} \dot{N}_{ji}^m - \nu_{ij}^m \dot{N}_{ij}^m}{\nu_{ji}^m}. \quad (58)$$

Therefore, our clock noise reduction performance will ultimately be limited by this modulation noise. To achieve the required performance, we must remove the higher modulation noise contributions from the right hand-sided modulation signals.

To remove these higher modulation noise terms, we need to measure the difference  $\Delta M_i$  of the two modulation signals on each spacecraft  $i$ . It can be measured electrically before the optical modulations are performed, or optically, using the sideband-sideband beatnotes in the reference interferometers.

We study here the second option, and define

$$\Delta M_i = \frac{\text{ref}_{ik,\text{sb}} - \text{ref}_{ik}}{2} - \frac{\text{ref}_{ij,\text{sb}} - \text{ref}_{ij}}{2}, \quad (59)$$

where the indices  $i, j, k \in \mathcal{I}_3^+$ .

These expressions are free of laser noise. Inserting eqs. (20a) and (20b), we see that they contain the modulation noise terms

$$\Delta M_i \approx \nu_{ij}^m N_{ij}^m - \nu_{ik}^m N_{ik}^m. \quad (60)$$

Note that both terms in eq. (59) contain the same information. We use here interferometric measurements from both adjacent MOSAs  $ij$  and  $ik$  to reduce the overall readout noise in  $\Delta M_i$ , which is uncorrelated in both measurements.

We now define

$$r_{ij}^c = r_{ij} + \frac{\dot{\mathbf{D}}_{ij} \Delta M_j}{\nu_{ji}^m}, \quad (61a)$$

$$r_{ik}^c = r_{ik} - \frac{\Delta M_i}{\nu_{ki}^m}, \quad (61b)$$

which contain the same differential clock noise as  $r_{ij}$  and  $r_{ik}$ , so that we can use them in place of the latter in the clock-noise reduction procedure described in section III. However, substituting previous expressions, it becomes clear that these terms do not contain modulation noise from right-handed MOSAs, as we have

$$r_{ij}^c = \frac{\dot{\mathbf{D}}_{ij} \nu_{jk}^m N_{jk}^m - \nu_{ij}^m N_{ij}^m}{\nu_{ji}^m}, \quad (62a)$$

$$r_{ik}^c = \frac{\dot{\mathbf{D}}_{ik} \nu_{ki}^m N_{ki}^m - \nu_{ij}^m N_{ij}^m}{\nu_{ki}^m}. \quad (62b)$$

Since we choose  $\nu_{ij}^m$  identical on on all left-handed MOSAs, this simplifies to

$$r_{ij}^c = \dot{\mathbf{D}}_{ij} N_{jk}^m - N_{ij}^m, \quad (63a)$$

$$r_{ik}^c = \dot{\mathbf{D}}_{ik} N_{ki}^m - N_{ij}^m, \quad (63b)$$

The remaining left-sided modulation error terms enter eqs. (63a) and (63b) with the same pattern as clock noise in eq. (35). This extends to the clock noise correction term we subtract in eq. (39), such that the overall modulation noise exactly replaces the clock noise in the original TDI expression. As such, following eq. (27), their PSDs are given by

$$\sum_{i,j,k \in \mathcal{I}_3^+} \left| a_{ij} \tilde{\mathbf{P}}_{ij}(\omega) + a_{ji} \tilde{\mathbf{P}}_{ji}(\omega) - b_{ij} [\tilde{\mathbf{P}}_{ik}(\omega) - \tilde{\mathbf{P}}_{ki}(\omega) \tilde{\mathbf{D}}_{ki}(\omega)] \right|^2 S_{N^m}(\omega), \quad (64)$$

where we assume that modulation noise is uncorrelated but of equal PSD  $S_{N^m}(\omega)$  for all 2.4 GHz sidebands.

In the particular case of  $X_2$ , we get

$$16 \sin^2(2\omega L) \sin^2(\omega L) A_{X_2}(\omega) S_{N^m}(\omega), \quad (65)$$

with  $A_{X_2}$  as the same scaling factor as given in eq. (30),

$$A_{X_2}(\omega) = (a_{12} - a_{13})^2 + a_{21}^2 + a_{31}^2 - 4b_{12}(a_{12} - a_{13} - b_{12}) \sin^2(\omega L). \quad (66)$$

We see in fig. 3 that this model fits perfectly our numerical results.

## C. Calibration errors

The clock correction algorithm relies on accurate measurements of the large beatnote frequency offsets  $a_{ij}, b_{ij}$ . Therefore, the achievable clock correction will be limited to a level proportional to the fractional error in these coefficients. A simple model for the residual noise from this effect can be derived by replacing the coefficients  $a_{ij}, b_{ij}$  in eq. (29) with terms representing the calibration error in the respective variables.

In reality,  $a_{ij}, b_{ij}$  will be determined with respect to the frequency of the USO, such that large deterministic offsets in its frequency will affect their measured value. We neglected such offsets in our analytical study and simulation, but remark that they are typically at a level below  $10^{-6}$  for a space-qualified USO [17], such that the residual noise due to this effect is smaller than the one presented in section V A.

## D. Other effects

The clock-noise reduction algorithm presented here relies on the same principles as the laser-noise reduction

by the traditional TDI combinations. As such, any effect which limits the latter will also impact the former in a similar fashion. Examples of such effects include the flexing-filtering coupling discussed in [12], aliasing of power due to insufficient filtering at high frequencies, interpolation artifacts around the Nyquist frequency, or the so-called *ranging errors* due to uncertainties in the values of the delays to apply.

However, as seen in fig. 3, clock noise only needs to be reduced by around 4 orders of magnitude, whereas laser noise needs to be reduced by around 8 orders of magnitude<sup>6</sup>. Therefore, if these effects are sufficiently small to allow for laser noise reduction, they should automatically be sufficiently small to not impact the clock noise reduction.

### E. Comparison to other algorithms

In fig. 4, we compare the performance of our clock-noise reduction algorithm (blue curve) against that from [7] (plotted in yellow). In our notation system and replacing delay operators by their Doppler-delay counterparts, the former algorithm is given by

$$X_2^c = X_2 - (1 - \dot{\mathbf{D}}_{12131})K_{X_1}, \quad (67)$$

where  $K_{X_1}$  is the correcting expression for the first-generation Michelson,

$$\begin{aligned} K_{X_1} = & -\frac{b_{12}}{2} \left[ (1 - \dot{\mathbf{D}}_{121})(r_{13}^c + \dot{\mathbf{D}}_{21}r_{31}^c) \right. \\ & \left. + (1 - \dot{\mathbf{D}}_{131})(r_{12}^c + \dot{\mathbf{D}}_{12}r_{21}^c) \right] \\ & + a_{12}(r_{13}^c + \dot{\mathbf{D}}_{13}r_{31}^c) - a_{13}(r_{12}^c + \dot{\mathbf{D}}_{12}r_{21}^c) \\ & + a_{21}[r_{13}^c - (1 - \dot{\mathbf{D}}_{131})r_{12}^c + \dot{\mathbf{D}}_{13}r_{31}^c] \\ & - a_{31}[r_{12}^c - (1 - \dot{\mathbf{D}}_{121})r_{13}^c + \dot{\mathbf{D}}_{12}r_{21}^c]. \end{aligned} \quad (68)$$

We see that the former algorithm performs slightly better than the one proposed above, by about a factor of two in amplitude.

This difference in the performance is explained by the factorization used to build the second-generation correction from the first-generation version. The factorized delays are applied to the whole first generation expression, which partly accounts for the time-varying beatnote frequencies, leading to a lower residual. This is only valid under the assumption that Doppler-delay operators can be commuted. In our setup, this assumption is only an approximation, but the residual due to this effect (i.e., terms scaled by the commutator of two delay operators) is smaller than that due to time-varying beatnotes (i.e., arising from the commutator of beatnote frequencies and delay operators).

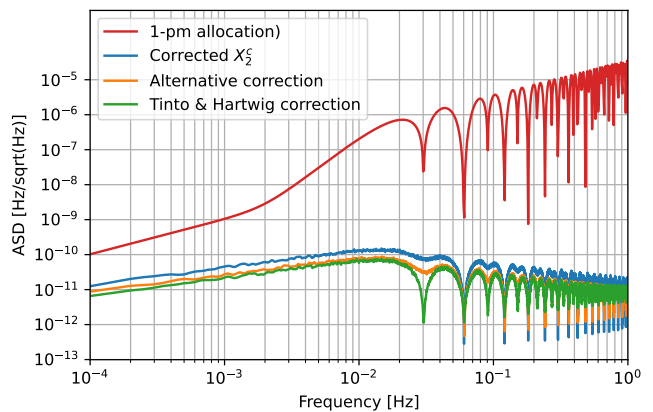


Figure 4. Comparison of the residual clock noise obtained with the reduction algorithm proposed in section III (in blue), Tinto & Hartwig’s algorithm from [7] (in yellow), and the alternative algorithm proposed in section V E (in green). The usual 1 pm-noise allocation curve is shown in red.

A first solution to achieve the same performance in the framework of this paper is to build the clock-noise correction for the first-generation Michelson  $X_1$  combination under the same assumptions, and then apply the same factor  $(1 - \dot{\mathbf{D}}_{12131})$ . Our simulations show that we exactly recover the same levels of residual clock noise. Note, however, that this solution only applies to TDI combinations which allow for such a factorization of the second-generation version.

A second, more general solution is to observe that beatnote frequencies always appear directly to the left of the clock noise terms in eq. (32). Going to eq. (33), we commuted the  $\mathbf{P}_{ij}$  with all beatnote frequencies. A more conservative approach would be to construct expressions  $R_{ij}^{a_{ij}}$  which evaluate to

$$R_{ij}^{a_{ij}} = \mathbf{P}_{ij} a_{ij} q_i, \quad (69)$$

and similarly for the other terms in eq. (32), such that they can be used directly in that equation. This can be approximated by directly rescaling all  $r_{ij}$  by  $a_{ij}$  before constructing  $R_{ij}$ . Inspecting our correction variable in eq. (35), one of the clock-noise terms always appears attached to a delay operator. This leaves us with a single delay-beatnote commutator in each  $r_{ij}$  term, due to the physical propagation delay. Note that this alternative approach can be applied to any TDI combination.

The results of this alternative scheme for  $X_2$  are presented in fig. 4 as the green dashed line. We don’t recover the exact zeros from [7] as they are related to the factor  $(1 - \dot{\mathbf{D}}_{12131})$ , but otherwise achieve a very similar residual noise level.

<sup>6</sup> For a laser noise of  $30 \text{ HzHz}^{-1/2}$  compared to the usual LISA 1 pm noise allocation curve.

## VI. CONCLUSION

In this article, we revisit the problem of clock-noise correction in space-based GW detectors. We find a general expression for the residual clock noise in any TDI variable, and provide a generic algorithm to reduce clock noise applicable to most TDI variables used in the literature.

We provide expressions for the residual clock noise levels after the correction, and show they are comparable to those previously proposed in the literature [7]. We study the effect time-varying beatnote frequencies have on these residuals and provide estimates of their magnitude. This effect was neglected in previous studies, and is limiting the residual clock noise with our simulation parameters.

These analytical results are backed up by time-domain simulations using the simulator LISA Instrument. In our studies, the spacecraft positions are simulated using numerical orbits provided by ESA, and the propagation delays are computed including relativistic corrections. In the analytical expressions, we assume that the beatnote frequencies, which are impacted by orbital mechanics, can be described as linear functions of time. This assumption yields excellent agreement with our simulation results.

In order to evaluate clock-noise suppression in comparison to other noise sources, we include a standard 1 pm noise allocation curve. We show that, using realistic values for the on-board USO, clock noise is dominating the overall noise level at low to mid frequencies if no clock-noise correction is performed. Using the algorithm we propose, the residual clock noise is suppressed significantly below the required level.

The clock-noise correction algorithm introduces a new modulation noise due to imperfections of the clock sidebands (used for the correction) with respect to the pilot tone (used as timing reference). We include these noise terms, as well as an algorithm to remove half of them using sideband beatnotes in the reference interferometers. We show that the remaining modulation noise is limiting the achievable noise suppression levels in the clock-corrected observables. Therefore, the signal chain from pilot tone to modulation sideband must fulfill strict timing requirements.

Future work on this topic could include a more realistic model for the clock behaviour, in particular accounting for large deterministic frequency offsets of the onboard oscillators.

TDI specific effects, such as flexing-filtering coupling, coupling of errors in the absolute ranging or in the interpolation scheme, could also be included in our model and simulations. However, their coupling to clock noise is expected to be much less relevant than their impact on the laser noise suppression, due to the much stricter suppression requirements for laser noise. Therefore, we do not expect them to significantly change the results presented here.

## Appendix A: Geometric TDI algorithm

We give here the algorithm presented in [18], updated to our notation and to include Doppler shifts. The starting point is a set of one-way measurements  $\eta_{ij} = \dot{\mathbf{D}}_{ij}p_j - p_i$ . To apply the algorithm, we also need the delay operators  $\dot{\mathbf{D}}_{ij}$  and their inverse advancement operators  $\dot{\mathbf{D}}_{-ij}$ , which fulfill

$$\dot{\mathbf{D}}_{ij}\dot{\mathbf{D}}_{-ji}x(t) = \dot{\mathbf{D}}_{-ji}\dot{\mathbf{D}}_{ij}x(t) = x(t), \quad (\text{A1})$$

for any function  $x(t)$ .

The goal is to construct a TDI combination which evaluates to

$$\text{TDI} = \dot{\mathbf{D}}_{\pm i_1 j_1} \dots \dot{\mathbf{D}}_{\pm i_n j_n} p_{j_n} - p_{i_1}, \quad (\text{A2})$$

where positive tuples of spacecraft indices  $(+i_k j_k)$  represent a delay while negative tuples  $(-i_k j_k)$  represent an advancement. In order to represent a valid interferometer, adjacent indices must fulfill  $j_k = i_{k+1}$ .

The algorithm can be summarized as follows:

1. Create a list of the desired time shifts as they appear in eq. (A2),

$$[\pm i_1 j_1, \dots, \pm i_n j_n]. \quad (\text{A3})$$

2. Create an empty list  $\mathcal{T}$  of delays/advancements, and initialize our TDI combination as  $\text{TDI} = 0$ .
3. Iterate through the list of time shifts, doing the following operations, assuming the indices are  $ij$ : if the entry is negative (i.e., an advancement), subtract

$$\text{TDI} \leftarrow \text{TDI} - \mathcal{T}\dot{\mathbf{D}}_{-ij}\eta_{ji}. \quad (\text{A4})$$

If the entry is positive (i.e., a delay), instead add

$$\text{TDI} \leftarrow \text{TDI} + \mathcal{T}\eta_{ij}. \quad (\text{A5})$$

Then, append either  $\dot{\mathbf{D}}_{-ij}$  or  $\dot{\mathbf{D}}_{ij}$  to  $\mathcal{T}$ .

4. Now, TDI evaluates to eq. (A2).

## ACKNOWLEDGMENTS

We are grateful to the members of the LISA Data Processing Group for their comments and help in improving the manuscript. In particular, we thank M. Muratore, G. Heinzel, A. Petiteau and M. Tinto for the fruitful discussions regarding this topic. We thank the referees for their help in improving the clarity of this manuscript. We also would like to thank M. Staab for reviewing the numerical implementation of this algorithm.

We gratefully acknowledge support by the Deutsches Zentrum für Luft- und Raumfahrt (DLR, German Space

Agency) with funding from the Federal Ministry for Economic Affairs and Energy based on a resolution of the German Bundestag (Project Ref. No. 50OQ1601 and 50OQ1801). This research has been supported by Centre National d'Études Spatiales (CNES), Centre National

pour la Recherche Scientifique (CNRS), Université Paris-Diderot, as well as the NASA Postdoctoral Fellowship program. The development of LISANode, LISA Instrument and PyTDI is part of the LISA Data Processing Group activities.

- 
- [1] P. Amaro-Seoane *et al.* (LISA Collaboration), *Laser Interferometer Space Antenna*, Tech. Rep. (ESA, 2017) arXiv.org:1702.00786 [astro-ph].
- [2] M. Armano *et al.*, Phys. Rev. Lett. **116**, 231101 (2016).
- [3] M. Armano *et al.*, Phys. Rev. Lett. **120**, 061101 (2018).
- [4] G. Weaver, J. Garstecki, and S. Reynolds, in *42nd Annual Precise Time and Time Interval (PTTI) Systems and Applications Meeting 2010* (2010) pp. 369–379.
- [5] S. Barke, *Inter-Spacecraft Frequency Distribution for Future Gravitational Wave Observatories*, Ph.D. thesis, Gottfried Wilhelm Leibniz Universität Hannover (2015).
- [6] R. W. Hellings, Phys. Rev. **D64**, 022002 (2001), arXiv:gr-qc/0012013 [gr-qc].
- [7] M. Tinto and O. Hartwig, Phys. Rev. D **98**, 042003 (2018).
- [8] M. Tinto and J. W. Armstrong, Phys. Rev. D **59**, 102003 (1999).
- [9] S. V. Dhurandhar, K. Rajesh Nayak, and J. Y. Vinet, Phys. Rev. D **65**, 102002 (2002), arXiv:gr-qc/0112059.
- [10] M. Vallisneri, Phys. Rev. D **71**, 022001 (2005), arXiv:gr-qc/0407102.
- [11] A. Petiteau, G. Auger, H. Halloin, O. Jeannin, E. Plagnol, S. Pireaux, T. Regimbau, and J.-Y. Vinet, Phys. Rev. D **77**, 023002 (2008), arXiv:0802.2023 [gr-qc].
- [12] J.-B. Bayle, M. Lilley, A. Petiteau, and H. Halloin, Phys. Rev. **D99**, 084023 (2019), arXiv:1811.01575 [astro-ph.IM].
- [13] M. Muratore, D. Vetrugno, and S. Vitale, Class. Quant. Grav. **37**, 185019 (2020), arXiv:2001.11221 [astro-ph.IM].
- [14] M. Tinto and S. V. Dhurandhar, Living Rev. Rel. **24**, 1 (2021).
- [15] J.-B. Bayle, O. Hartwig, and M. Staab, Phys. Rev. D (2021), arXiv:2103.06976 [gr-qc].
- [16] M. Otto, *Time-Delay Interferometry Simulations for the Laser Interferometer Space Antenna*, Ph.D. thesis, Gottfried Wilhelm Leibniz Universität Hannover (2015).
- [17] S. Asmar, “Ultra-stable oscillators for probe radio science investigations,” (2012), jet Propulsion Laboratory, California Institute of Technology, Pasadena CA, USA.
- [18] M. Vallisneri, Phys. Rev. **D72**, 042003 (2005), [Erratum: Phys. Rev.D76,109903(2007)], arXiv:gr-qc/0504145 [gr-qc].
- [19] J.-B. Bayle, *Simulation and Data Analysis for LISA : Instrumental Modeling, Time-Delay Interferometry, Noise-Reduction Performance Study, and Discrimination of Transient Gravitational Signals*, Ph.D. thesis, Paris U. VII, APC (2019).
- [20] S. Plaszczynski, Fluct. Noise Lett. **7**, R1 (2007), arXiv.org:0510081 [astro-ph].